Single-source precursor synthesis of quinary AgInGaZnS QDs with tunable photoluminescence emission

Perizat Galiyeva, Hervé Rinnert, Lavinia Balan, Halima Alem, Ghouti Medjahdi, Bolat Uralbekov, Raphaël Schneider

Single-source precursor synthesis of quinary AgInGaZnS QDs with tunable photoluminescence emission

Perizat Galiyeva [a], Hervé Rinnert [b], Lavinia Balan [c], Halima Alem [b], Ghouti Medjahdi [b], Bolat Uralbekov [d], Raphaël Schneider [a,*]

[a] *Université de Lorraine, CNRS, LRGP, F-54000 Nancy, France*

[b] *Université de Lorraine, CNRS, IJL, F-54000 Nancy, France*

[c] *CEMHTI-UPR 3079 CNRS, Site Haute Température, 1D avenue de la Recherche Scientifique, 45071 Orléans, France*

[d] *Al-Farabi Kazakh National University, Al-Farabi Av., 71, Almaty 050040, Kazakhstan*

Corresponding author: raphael.schneider@univ-lorraine.fr

Abstract. A single source molecular precursor synthesis of new quinary Ag-In-Ga-Zn-S (AIGZS) QDs is presented. Dithiocarbamate complexes with varied Ag/In/Ga/Zn ratios were prepared from $AgNO_3$, $In(NO_3)_3$, $Ga(NO_3)_3$ and Zn(diethyldithiocarbamate)$_2$. The thermal decomposition of these complexes at 220°C in oleylamine produces AIGZS QDs emitting from the visible to the near-infrared region and with photoluminescence quantum yields (PL QYs) up to 48.3%. For AIGZS QDs prepared with a (Ag + In + Ga)/Zn molar ratio of 1, intragap states likely involving Ag^+ ions are responsible of the PL emission and the PL lifetime could reach 278 ns. A marked increase of the PL lifetime (up to 915 ns) was observed when decreasing the (Ag + In + Ga)/Zn molar ratio to 0.5. The optical properties of AIGZS QDs could be maintained after transfer in aqueous solution. AIGZS should be of high potential for various applications due to their PL emission tunability and high PL QYs.

Keywords: AgInGaZnS quantum dots; single source precursor synthesis; dithiocarbamate complexes; photoluminescence

1. Introduction

Ternary I-III-VI_2 semiconductor quantum dots (QDs) (where I = Ag or Cu, III = In or Ga and VI = S, Se or Te) and quaternary ones of general formula I-II-III-VI_2 (where II = Zn) obtained after shelling and alloying with ZnS have widely been investigated in recent years due to their unique chemical and optical properties [1-5]. Many studies on these QDs have been limited to the direct bandgap $CuInS_2$/ZnS (CIZS) [6,7] and $AgInS_2$/ZnS (AIZS) [8-10] semiconductors that have been demonstrated to be highly promising for photovoltaic or photocatalytic applications [11-13], solid-state lighting devices [14-16] or bio-imaging [17,18]. Moreover, these QDs are considered to be safe and environmentally benign as they do not contain toxic elements such as Cd or Pb.

One of the key advantages of I-II-III-VI_2 QDs is their high degree of compositional flexibility by varying monovalent and/or trivalent cations which allows to finely tune their bandgap energy and thus the photoluminescence (PL) emission wavelength over all the whole visible region and even in the near infrared [1-5]. In recent years, various quaternary compositional and structural variants such as green to orange emitting $CuInGaS_2$ [19,20], green to red emitting $CuGaZnS_2$ [21] or $CuGaZnSe_2$ [22], blue to orange emitting Mn^{2+}-doped $CuGaZnS_2$ [23,24], violet to aqua emitting $AgGaZnS_2$ [25,26] or blue to orange-emitting $AgGaInS_2$ [27,28] have been reported. Only one report describes the synthesis of quinary $CuGaInZnS_2$ QDs [19]. The PL emission of these dots was demonstrated to be tunable from the orange to the red by varying the Cu/Ga molar ratio. The synthesis of previously mentioned quaternary and quinary nanocrystals is classically performed like that of AIZS and CIZS QDs by thermal decomposition of metal salts or organometallic precursors in the presence of S or Se precursors using dodecanethiol, oleylamine (OAm) or ethylenediamine as capping ligand [19-26,28]. $AgInS_2$ QDs were also used as template to prepare $AgGaInS_2$ by cation exchange between In^{3+} and Ga^{3+} [27]. Some of the synthetic protocols require the injection of Na_2S or NaHSe, multiple injections of the shell precursors (generally ZnS or ZnSe) or the handling of air-sensitive reagents.

In recent years, single-source molecular precursor synthesis of QDs has emerged due to its simplicity and safety when compared to multi-step processes [29-32]. In this context, transition metal dithiocarbamates are well known to decompose under inert atmosphere into metal sulfide nanocrystals [33]. This approach has successfully been used to prepare binary like Ag_2S, ZnS or CdS, ternary like $Zn_{1-x}Mn_xS$ or $Zn_xCd_{1-x}S$ nanocrystals using a mixture of dithiocarbamates of each of these metals [33-37]. However, the use of a single

dithiocarbamate complex containing more than one metal for the production of corresponding sulfides is far unexplored. Herein, a facile method allowing the production of highly fluorescent AgInGaZnS (AIGZS) QDs with PL quantum yields (PL QY) up to 48.3% is presented. Using a single dithiocarbamate complex of Ag^{+}, In^{3+}, Ga^{3+} and Zn^{2+} and OAm as solvent and capping ligand, a series of AIGZS QDs could be produced by varying the Ag/In/Ga/Zn ratio in the precursor. The obtained QDs exhibit a low size (ca. 2 nm) and their PL emission could be tuned from the visible to the near-infrared. Moreover, the optical properties could be maintained after ligand exchange and transfer into water.

2. Experimental

2.1. Materials

Silver nitrate $AgNO_3$ (ReagentPlus, >99%, Sigma), gallium nitrate hydrate $Ga(NO_3)_3.xH_2O$ (>99.9%, Sigma), indium nitrate hydrate $In(NO_3)_3.xH_2O$ (>99.9%, Alfa Aesar), zinc diethyldithiocarbamate $Zn(DDTC)_2$ (97%, Sigma), sodium diethyldithiocarbamate NaDDTC (ACS reagent, Sigma), oleylamine OAm (80-90%, Acros), glutathione GSH (99%, Sigma), tetramethylammonium hydroxide pentahydrate (97%, Sigma), glycine (99+%, Acros), carbon disulfide (>99.9%, Sigma) were used as received without any purification.

2.2. Preparation of $Ag_xIn_yGa_{2-x-y}Zn_2(S_2CN(C_2H_5)_2)_4$ precursors

A representative synthetic protocol for AIGZS QDs prepared with a Ag/In/Ga/Zn molar ratio of 1/0.5/0.5/2 is given. $AgNO_3$ (1 mmol), $In(NO_3)_3$ (0.5 mmol) and $Ga(NO_3)_3$ (0.5 mmol) were mixed with $Zn(DDTC)_2$ (2 mmol) in 10 mL of a 1:1 water-methanol mixture. The solution was stirred for 2 h at room temperature to form $Ag_xIn_yGa_{2-x-y}Zn_2(S_2CN(C_2H_5)_2)_4$ precursors (the (Ag + In + Ga)/Zn molar ratio is of 1). The product was collected by centrifugation (4000 rpm for 15 min), dried under vacuum and stored at 4°C before use.

2.3. Preparation of Ag-In-Ga-Zn-S (AIGZS) QDs

The AIGZS QDs were synthesized by thermolysis of $Ag_xIn_yGa_{2-x-y}Zn_2(S_2CN(C_2H_5)_2)_4$ precursors in oleylamine (OAm). First, the dried precursor (100 mg) was dispersed in OAm (6 mL) and the mixture was stirred under argon flow until homogenization. Then, the solution was heated (190, 220 or 250°C) for 10 min and the color changed to dark. After cooling, the large sized crystals were removed by centrifugation (5000 rpm for 10 min). The supernatant was precipitated by adding an excess of methanol and the powder was collected by centrifugation (5000 rpm for 10 min) and dried under vacuum. Next, the dried product was redispersed in OAm (6 mL) and the solution was heated (190, 220 or 250°C) for 30 min. The obtained AIGZS QDs were precipitated by adding an excess of methanol, recovered by centrifugation (5000 rpm for 10 min) and purified by washing with methanol.

2.4. Transfer of AIGZS QDs into water

2.4.1. Glutathione tetramethylammonium (GTMA) coating

GTMA-coating was conducted using a previously described method [38]. Briefly, GTMA was prepared by dissolving GSH (30 mg) and TMAH (54 mg) in 1 mL of methanol. Separately, 5 mg of AIGZS@OAm QDs were dispersed in 1 mL toluene, then 5 mL chloroform was added. Next, 0.5 mL of GTMA solution was dropwise added to the QDs solution and the mixture was vigorously stirred for 15 min. Then, water (4.5 mL) was added and the two-layer mixture was slightly shaken to transfer QDs into the water layer before being left for 1 h to reach equilibrium. Finally, the top water layer containing GTMA-capped AIGZS QDs was collected.

2.4.2. Glycine diethyldithiocarbamate (Gly-DDTC) capping [39]

AIGZS@OAm QDs (2 mg) dispersed in a methanol/chloroform mixture (3 mL, 1:1 vol.) were added to glycine (80 mg) in a methanol/chloroform mixture (2 mL, 1:1 vol.) containing TMAH (384.2 mg) and CS_2 (81 mg). The mixture was stirred for 12 h at room temperature followed by centrifugation for 3 min at 4000 rpm. Then, 5 mL of diethyl ether were added to the supernatant and the mixture centrifuged for 10 min at 5000 rpm. Next, the fluorescent bottom layer was dispersed in methanol (2 mL), precipitated with THF (5 mL) and centrifuged (5000 rpm, 10 min). The obtained solid was dispersed in Tris buffer (0.1 M, pH 8.5).

2.5. Characterization

The morphology of the QDs was investigated by transmission electron microscopy (TEM) and high-resolution TEM (HR-TEM) using a Philips CM200 instrument operating at 200 kV. A drop of the QDs dispersed in toluene was deposited onto a carbon-coated copper grid. The crystal structure of AIGZS QDs was examined by X-ray diffraction (XRD) using a Panalytical X'Pert Pro MPD diffractometer with Cu Kα radiation (λ = 0.15418 nm). The dried samples were placed on a silicon zero-background sample holder and the XRD patterns were recorded at room temperature. XRD patterns were analyzed using TOPAS (Bruker AXS, Version 4-2). X-ray photoelectron spectroscopy (XPS) measurements were carried out with a Gammadata Scienta SES 200-2 spectrometer. Thermogravimetric analysis (TGA) was conducted under air atmosphere from room temperature to 800°C at a heating rate of 10°C/min using a TGA/DSC1 STAR equipment (MettlerToledo). Inductively Coupled Plasma-Optical Emission Spectrometer (ICP-OES) measurements were conducted on a Varian 720-ES equipment. Hydrodynamic QDs sizes and Zeta potential measurements were determined by dynamic light scattering (DLS) on a Zetasizer Nano ZS (green laser beam 532 nm) (Malvern).

Fourier transform infrared (FT-IR) spectra were collected on a Brucker ALPHA spectrometer. Optical absorption and PL emission spectra were recorded on a UV-visible absorption spectrometer (Thermo Scientific Evolution 220) and spectrofluorometer (Horiba Fluoromax-4 Jobin Yvon), respectively. PL spectra were spectrally corrected and PL QYs were determined relative to Rhodamine 6G in ethanol (PL QY = 94%). For the time resolved photoluminescence (TR-PL) experiments, the QDs were pumped by the 355 nm line of a frequency-tripled YAG (yttrium aluminium garnet):Nd laser. The laser pulse frequency, energy and duration were typically equal to 10 Hz, 50 µJ and 10 ns, respectively. The PL signal was analysed by a monochromator equipped with a 600 grooves/mm grating and by a photomultiplier tube cooled at 190 K. The rise time of the detector is equal to around 3 ns.

3. Results and discussion

3.1. Synthesis and optical properties of AIGZS QDs

The AIGZS QDs precursors were prepared by mixing $AgNO_3$, $Ga(NO_3)_3$ and $In(NO_3)_3$ with $Zn(DDTC)_2$ ($nAg^+ + nIn^{3+} + nGa^{3+}/nZn^{2+} = 1$ or 0.5) in a water/methanol mixture (Scheme 1).

The powders obtained after centrifugation and drying were stored at 4°C before use and can be handled in open air without any protection. The thermolysis of the precursors in the presence of OAm produces AIGZS QDs, DDTC serving as sulfur source and OAm as capping ligand.

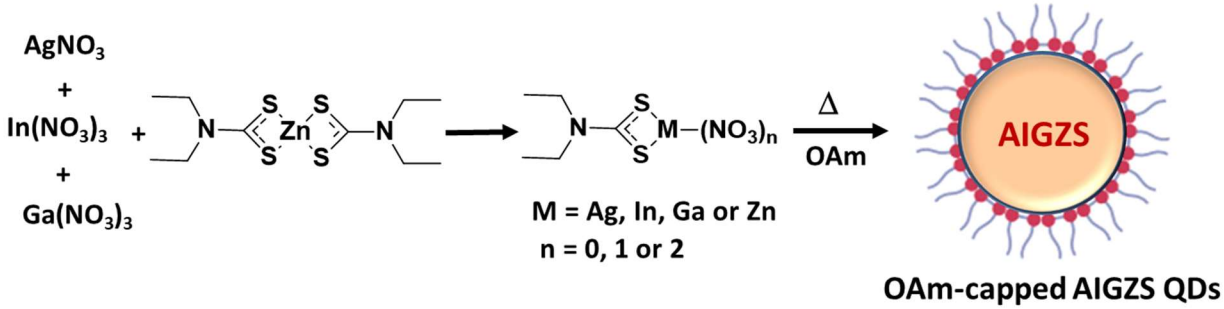

Scheme 1. Schematic representation of AIGZS QDs synthesis.

According to the hard and soft acids and bases theory, Ag^+ is a soft Lewis acid, Ga^{3+} and In^{3+} are hard Lewis acids while Zn^{2+} can be considered as borderline [40]. The reaction of $Zn(DDTC)_2$ with $AgNO_3$, $Ga(NO_3)_3$ and $In(NO_3)_3$ should favor the exchange of Zn^{2+} by Ag^+ as DDTC is a soft base. Once dispersed in OAm, In^{3+} and Ga^{3+} likely coordinate more strongly with OAm which is a harder Lewis acid. ICP-OES and XPS analyses conducted on AIGZS QDs indicate that the Ag/In/Ga/Zn ratio is close to the feeding ratio used to prepare the precursors (*vide infra*), suggesting that all metal cations incorporate well in the precursors either as mono-, bis- or tris-complexes of DDTC.

The cation exchange between Ag, In and Ga nitrates and $Zn(DDTC)_2$ during the $Ag_xIn_yGa_{2-x-y}Zn_2(S_2CN(C_2H_5)_2)_4$ precursors synthesis was first evidenced by TGA. Pure $Zn(DDTC)_2$ is stable until ca. 250°C and a sharp weight loss is observed above 300°C, which corresponds to the decomposition of $Zn(DDTC)_2$ into ZnS (Fig. S1). For all precursors, the decomposition is more complex and takes place in successive steps between 100 and 300°C. The remaining mass (ca. 35%) is higher than that measured after thermolysis of $Zn(DDTC)_2$ (ca. 10%), indicating the formation of higher molecular weight metal sulfides. The precursors powders were also examined by XRD. While pure $Zn(DDTC)_2$ exhibits a monoclinic structure (JCPDS No 44-1815) [41], new signals appear in the XRD patterns of the precursors, further confirming that a reaction occurred between $Zn(DDTC)_2$ and Ag, In and Ga nitrates (Fig. S2).

The FT-IR spectra of the precursors show signals at ca. 3360 cm^{-1} (γ_{O-H} from adsorbed water molecules), 2967-2867 cm^{-1} (γ_{C-H}), 1638 cm^{-1} (δ_{O-H}) and numerous signals between 1497 and 1270 cm^{-1} originating from C-H and C-N stretching modes (Fig. S3) [42]. The signals at 1204, 1134 and 1057 cm^{-1} can be attributed to γ_{C-S}, γ_{N-CS2} and $\gamma_{C=S}$ bonds, respectively [42]. The weak signals below 500 cm^{-1} originate from metal-S bonds. All these signals disappear after heating at 220°C and only the characteristic vibrations of the OAm ligand can be observed for AIGZS QDs (γ_{N-H} at 3212 cm^{-1}, γ_{C-H} at 2935 and 2848 cm^{-1}, δ_{N-H} and NH_2 scissoring at 1624 cm^{-1}, γ_{C-C} at 1456 cm^{-1}, and $\delta_{=C-H}$ in plane and out of plane at 1039 and 961 cm^{-1}, respectively) (Fig. S4). Some additional signals between 1000 and 500 cm^{-1} originate from N-H wagging modes and δ_{C-H}. Finally, it can also be noted that depending on the Ag/In/Ga/Zn ratio, the precursors absorb in the UV and in the visible region until ca. 450 nm (see Fig. S5 for representative UV-visible absorption spectra). After thermolysis, the absorption in the visible region is significantly extended, which further confirms the decomposition of the precursors into AIGZS QDs.

In preliminary experiments conducted with the precursor prepared with a Ag/In/Ga/Zn ratio of 0.5/1/0.5/2, we varied the temperature during the preparation of AIGZS QDs (190, 220 or 250°C). A gradual redshift of the PL emission wavelength was observed with the increase of the temperature (560, 583 and 601 nm for reactions carried out at 190, 220 and 250°C, respectively), likely due to an increase of the nanocrystals size (Fig. 1a). The highest PL QY (11%) was measured for nanocrystals prepared at 220°C and this temperature was kept in further experiments.

After heating at 220°C for 10 min (step 1), some aggregates formed in the reaction flask. These large sized particles were removed by centrifugation and the AIGZS QDs contained in the supernatant were re-heated at 220°C in the presence of OAm (step 2). A red-shift of the PL emission from 570 to 583 nm was observed after 10 min of heating and extending the heating period had no further influence of the PL emission peak (Fig. 1b). A marked increase of the PL QY from 11 to 20.2% was also observed after the second heating at 220°C, suggesting an improvement of nanocrystals surface passivation by OAm and the removal of surface defects that may serve as nonradiative channels. Finally, TGA analysis of the dots shows only one weight loss starting at ca. 250°C, likely originating from the removal of the OAm capping ligand (Fig. S1). The remaining mass is of ca. 80%, which confirms that AIGZS QDs are covered by a thick OAm shell.

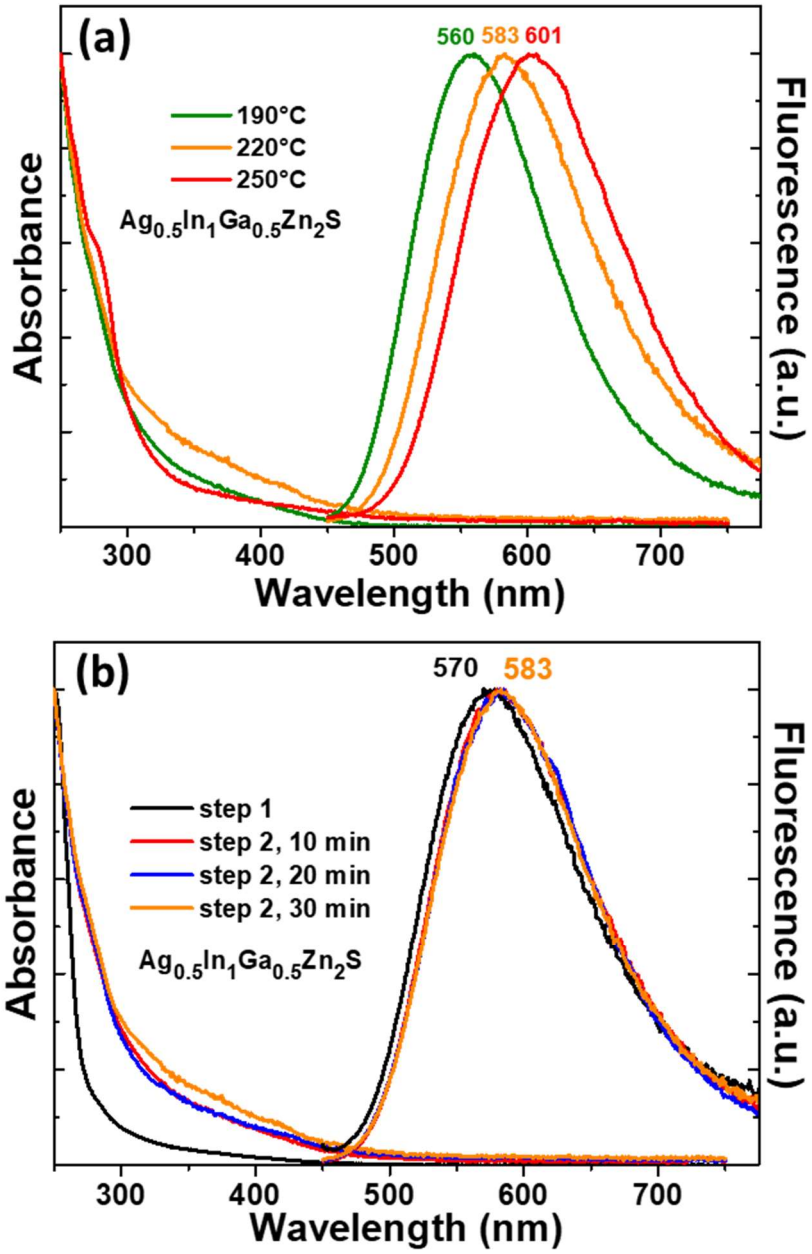

Fig. 1 UV-visible and normalized PL emission spectra of AIGZS QDs (a) when varying the heating temperature and (b) after a first heating at 220°C and after a second heating at the same temperature.

Fig. 2a-b show the evolution of UV-visible absorption and PL emission spectra of AIGZS QDS dispersed in chloroform. All absorption spectra exhibit almost similar features regardless of the Ag/In/Ga/Zn ratio. A relatively well resolved absorption peak can be observed at ca. 290 nm and all QDs absorb in the visible region up to ca. 550 nm. However, no marked exciton

peak can be observed in the visible region likely due to the distribution of vibrational states in AIGZS QDs, which is a common feature for ternary or quaternary QDs [9,10]. The steady state PL emission spectra are broad with a full-width at half-maximum (fwhm) varying between 131 and 170 nm, which is characteristic of donor-acceptor (D-A) transitions and trap-state emissions (*vide infra*) [9,10].

We first varied the Ag/In/Ga ratio without altering the amount of $Zn(DDTC)_2$ (nAg + In + Ga/nZn = 1). Only the nanocrystals prepared with a low Ag content (ratio of 0.25/0.875/0.75/2) exhibit a strong emission located at 515 nm associated to a defect related emission at lower energy. For all other dots, a single component emission was observed. A redshift of the PL emission from 515 to 650 nm can be observed with the increase of the Ag content due to the lower bandgap of Ag_2S (0.85-1.1 eV) [43] compared to In_2S_3 (1.98-2.2 eV) [44] and Ga_2S_3 (ca. 3.4 eV) [45] in the bulk state (Fig. 2b-c). Next, by decreasing the Zn content (nAg + In + Ga/nZn = 0.5), a significant redshift of the PL emission to 699 nm was observed due to the lower contribution of the wide bandgap ZnS material (3.6 eV). These results indicate that the PL emission can be tailored by changing the Ag/In/Ga/Zn ratio. It should be noted that the metal/S ratio was also modified during this experiment as DTTC serves as sulfur source. By maintaining the S concentration by addition of NaDDTC, the PL emission wavelength is further shifted to 716 nm. The bandgap values were determined from the Tauc plots of $(\alpha h\nu)^2$ vs. hv (where α is the absorption coefficient and hv is the photon energy) and were found to decrease from 2.94 to 2.08 eV (Fig. S6).

The characteristic optical properties of AIGZS QDs, namely the broad PL emission with a large Stokes shift, are typical of ternary and quaternary semiconductor nanocrystals and originate from surface states (vacancies and dangling bonds) and interstitial states (interstitial atoms and vacancies) that usually dominate the PL emission. The changes of the PL emission wavelength observed when varying the Ag/In/Ga/Zn ratio result from the lower bandgap of Ag-richer AIGZS QDs and from the wider bandgap of In, Ga or Zn-rich AIGZS QDs and thus from the shift of the intragap donor and acceptor levels. As can be seen from Table 1, the PL QY of AIGZS QDs increases with the Ag content of the nanocrystals. The highest PL QYs were measured for AIGZS QDs prepared with Ag/In/Ga/Zn ratios of 0.66/0.66/0.66/2 and 1/0.5/0.5/2 (48.3 and 47.8%, respectively, entries d and e). These results suggest that Ag vacancies and Ag interstitials play a key role in the PL mechanism as previously observed for AIS and AIZS QDs [9,10]. Contrary to PL QY values determined for Ag-In-Ga-S or Cu-In-Ga-Zn-S

QDs [20], the increase of the Ga content in AIGZS QDs was found to be less deleterious than that of In (compare entries b and c). A decrease of the PL QY (25.4%) was also observed with the decrease of the Zn and S loading in AIGZS QDs (entry f). A similar PL QY (23.6%) was determined when adding NaDDTC in the reaction medium, indicating that the decrease was linked to the Zn loading (entry g).

Finally, we also compared the optical properties of AIGZS QDs prepared using the $Ag_xIn_yGa_{2-x-y}Zn_2(S_2CN(C_2H_5)_2)_4$ precursors to those of nanocrystals obtained by reacting $AgNO_3$, $Ga(NO_3)_3$, $In(NO_3)_3$ and $Zn(DDTC)_2$ in OAm at 220°C. UV-visible absorption and PL emission spectra of the dots prepared without using the precursor and with a Ag/In/Ga/Zn molar ratio of 1/0.5/0.5/2 are shown in Fig. S7. A marked blue shift of the PL emission (575 nm vs 650 nm for QDs prepared using the precursor) and a strong decrease of the PL QY (5.9% vs 47.8%) were observed. These results demonstrate the value of using the $Ag_xIn_yGa_{2-x-y}Zn_2(S_2CN(C_2H_5)_2)_4$ precursor for the preparation of AIGZS QDs.

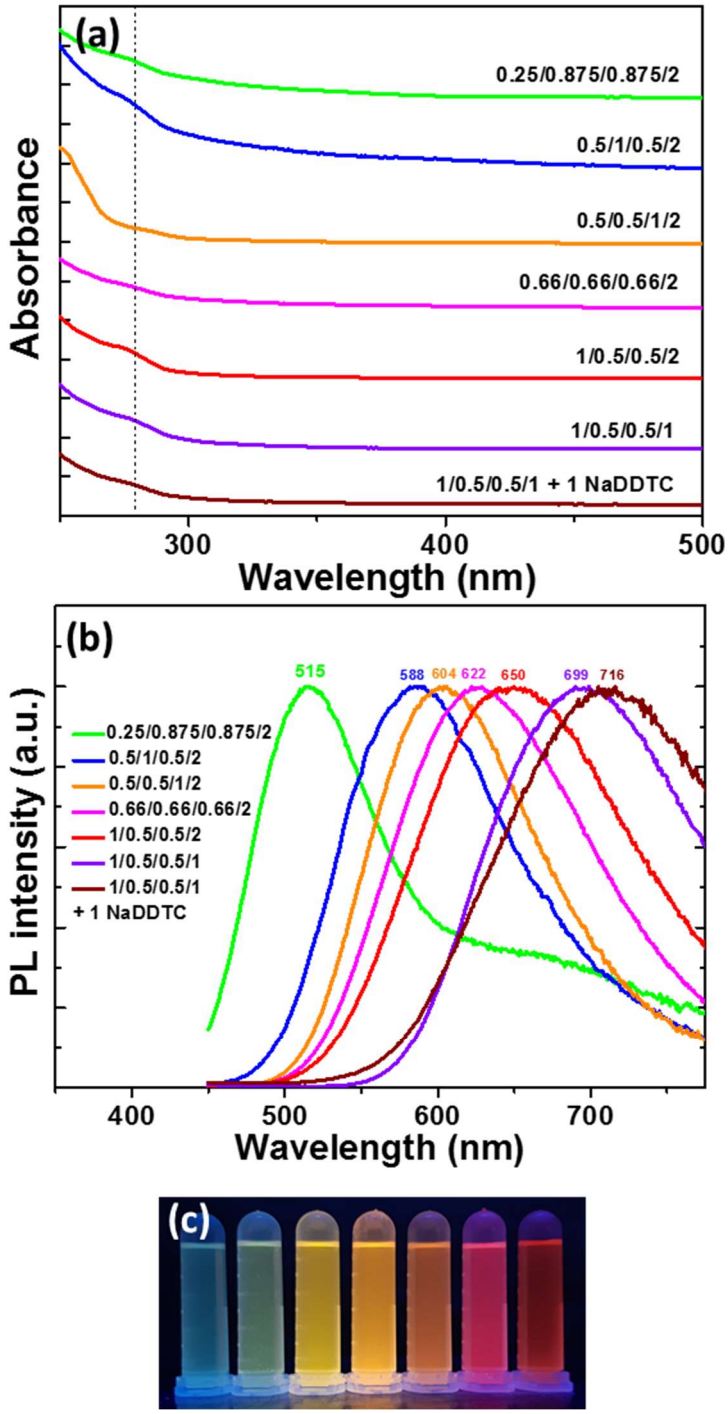

Fig. 2. (a) UV-visible and (b) normalized PL emission spectra of AIGZS QDs when varying the Ag/In/Ga/Zn ratio, and (c) digital photograph of the dots under UV light illumination.

Table 1. PL QYs, time constant τ_1 and τ_2 and the contributions of decays A_1 and A_2 of AIGZS QDs when varying the Ag/In/Ga/Zn ratio.

Entry	Ag/In/Ga/Zn ratio	PL QY (%)[a]	A_1	τ_1 (ns)	A_2	τ_2 (ns)	τ_{av} (ns)
a	0.25/0.875/0.875/2	14.3	0.828	66.3	0.171	262.3	99.9
b	0.5/1/0.5/2	20.2	0.679	52.9	0.320	228.7	109.3
c	0.5/0.5/1/2	41.9	0.681	143.5	0.318	549.3	272.6
d	0.66/0.66/0.66/2	48.3	0.590	121.6	0.409	505.1	278.8
e	1/0.5/0.5/2	47.8	0.628	116.6	0.371	521.1	226.3
f	1/0.5/0.5/1	25.4	0.663	189.9	0.336	883.3	423.3
g	1/0.5/0.5/1 + 1 NaDDTC	23.6	0.494	424.9	0.505	1395.7	915.3

[a] Determined using chloroform as solvent.

To investigate the dynamic properties of photo-generated electron/hole pairs, time-resolved decays of AIGZS QDs at the maximum emission wavelength were measured (Fig. 3). The data were best fitted using a bi-exponential function $I(t) = A_1 \exp(-t/\tau_1)$ and $A_2 \exp(-t/\tau_2)$ where τ_1 and τ_2 are the time constants of the PL and A_1 and A_2 the normalized amplitudes of the components. The average lifetime τ_{av} was determined using the formula $\tau_{av} = (A_1\tau_1 + A_2\tau_2)/(A_1 + A_2)$. The time constants and fitting parameters are listed in Table 1. Two radiative channels were observed. The fast decay component τ_1 is attributed to surface trap state recombination and the slow decay component τ_2 to the recombination of electrons via defect states located within the bandgap (D-A recombination) [9,10,46-48]. AIGZS QDs prepared with the Ag/In/Ga/Zn ratio of 0.25/0.875/0.875/2 exhibit the shortest PL lifetime (99.9 ns) due to the high contribution of surface defects. For QDs prepared with a stoechiometric ratio of (Ag + In + Ga)/Zn of 1, τ_{av} is the highest (278.8 ns) when equimolar amounts of Ag, In and Ga are used for their synthesis (entry c). This long PL decay is characteristic of radiative recombinations involving intragap states of QDs exhibiting inherent lattice defects [9,10]. The highest A_2 contributions were determined for AIGZS QDs prepared with Ag/In/Ga/Zn ratios of 0.66/0.66/0.66/2 and 1/0.5/0.5/2, which is in good agreement with the PL QYs of these dots (entries d and e). For QDs prepared with a (Ag + In + Ga)/Zn molar ratio of 0.5, a marked

increase of τ_1 and τ_2 is observed and τ_{av} reaches 915 ns (entry g), suggesting that new surface and lattice defects generated by the default in Zn^{2+} ions could be involved in the transitions.

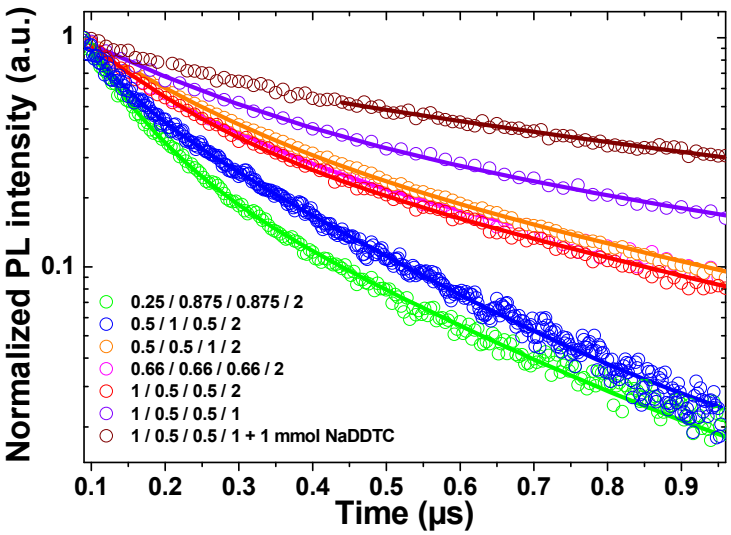

Fig. 3. Time resolved decay profiles of AIGZS QDs recorded at the maximum emission wavelength.

3.2. Characterization of AIGZS QDs

The crystal structure, the size and the size distribution of AIGZS QDs were studied by XRD, TEM and selected area diffraction (SAED). The reflection peaks are characteristic of a tetragonal chalcopyrite phase and their broadness is indicative of the small size of the nanocrystals (Fig. 4a). The mean crystalline size, calculated from the (112) reflection by the Scherrer formula, is of ca. 2 nm. It can also be observed that changes in the Ag/In/Ga/Zn ratio do not affect the crystalline structure of the dots. Finally, no diffraction peaks of Ag_2S, In_2S_3, Ga_2S_3 or ZnS could be observed in the XRD patterns, indicating the high purity of AIGZS QDs.

A representative TEM image of AIGZS QDs prepared with a Ag/In/Ga/Zn ratio of 1/0.5/0.5/2 is shown in Fig. 4b (see Fig. S8 for the TEM images of all QDs prepared). Regardless of the Ag/In/Ga/Zn ratio used for the synthesis of the precursors, AIGZS QDs exhibit a spherical shape and a relatively narrow size distribution (2.0 ± 0.4 nm). The clear lattice planes observed in the HR-TEM image (Fig. 4c) and the electron diffraction pattern (inset of Fig. 4b) confirm their good crystallinity. The lattice spacing of 0.31 nm is consistent with the (112) plane of the tetragonal structure (JCPDS No 04-021-8345, space group I-42d). The EDX analysis shows the

characteristic peaks of Ag, In, Ga and Zn (Fig. S9). The atomic ratio Ag/In/Ga/Zn is 1.03/0.47/0.5/2, value close to the feeding ratio, which confirms that all metals are well incorporated in the QDs.

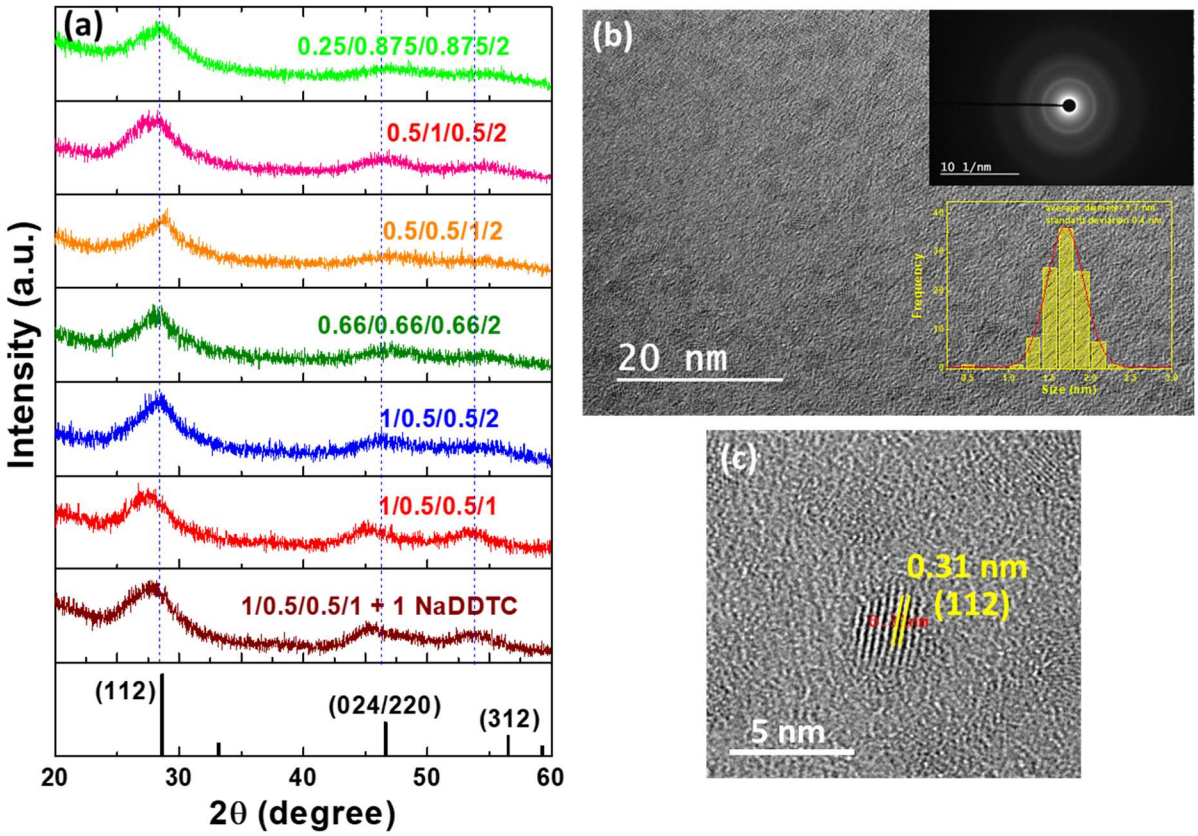

Fig. 4. (a) XRD patterns of AIGZS QDs, (b) TEM image and (c) HR-TEM image of AIGZS QDs prepared with a Ag/In/Ga/Zn ratio of 1/0.5/0.5/2. The insets of (b) are the SAED pattern and the size distribution.

To determine the accurate composition of AIGZS QDs, the samples were characterized by ICP-OES and the results are described in Table 2. As previously observed by EDX, the composition of the dots is consistent with the nominal Ag/In/Ga/Zn ratio of the precursors. These results further demonstrate that Ag, In, Ga and Zn elements in the various precursors synthesized participate uniformly in the nucleation and growth and that the synthetic route developed allows the preparation of composition controlled AIGZS QDs.

Table 2. Theoretical and experimental composition of AIGZS QDs.

Theoretical Ag/In/Ga/Zn ratio	Ag/In/Ga/Zn ratio determined by ICP-OES[a]
0.25/0.875/0.875/2	0.27/0.83/0.90/2
0.5/1/0.5/2	0.51/0.97/0.52/2
0.5/0.5/1/2	0.53/0.46/1.01/2
0.66/0.66/0.66/2	0.68/0.65/0.67/2
1/0.5/0.5/2	1.01/0.51/0.48/2
1/0.5/0.5/1	1.03/0.48/0.49/1

[a] Results were normalized to the Zn content of AIGZS QDs.

XPS was also used to investigate the chemical state and the composition of AIGZS QDs. The XPS survey spectrum shows the presence of Ag, In, Ga, Zn and S elements along with C and N originating from the OAm capping ligand (Fig. S10). The signals at 367.67, 445.04, 452.57, 1118.26 and 1021.79 eV can be assigned to Ag $3d_{5/2}$, In $3d_{5/2}$, In $3d_{3/2}$, Ga $2p_{3/2}$ and Zn $2p_{3/2}$, respectively, and confirm the valence states of Ag^{+}, In^{3+}, Ga^{3+} and Zn^{2+}. The deconvoluted signals at 161.49 and 162.69 eV correspond to S $2p_{3/2}$ and S $2p_{1/2}$, respectively, indicating that the metal cations are associated to S^{2-}.

3.3. Aqueous phase transfer of AIGZS QDs

After post-preparation treatments and removal of unreacted precursors, AIGZS QDs were successfully transferred into aqueous phase via exchange of the hydrophobic OAm ligand with glutathione tetramethylammonium (GTMA) or glycine dithiocarbamate (Gly-DTC) (Fig. 5) [38,39].

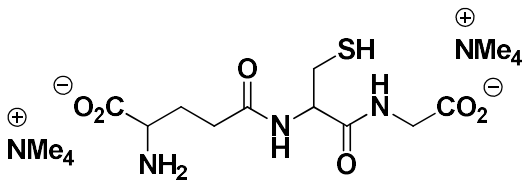

GTMA

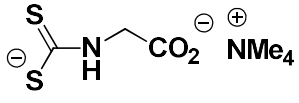

Gly-DDTC

Fig. 5. Structures of GTMA and Gly-DDTC ligands used to transfer AIGZS QDs into aqueous solution.

The thiol function of GTMA and the dithiocarbamate function of Gly-DTC enable the removal of the OAm ligand and convert the native oil soluble nanocrystals into hydrophilic ones (Fig. 6a). Fig. 6b shows the UV-visible and the PL emission spectra before and after the ligand exchange. No significant changes could be observed in the UV-visible spectrum of AIGZS@GTMA QDs compared to the native dots. For Gly-DTC, a strong and well resolved peak appears at ca. 305 nm, which indicates that the dots are well capped by the dithiocarbamate bearing ligand. This was further confirmed by the FT-IR spectrum of Gly-DTC capped QDs which shows the characteristic signal of γ(N-H) at 3374 cm^{-1} (associated to γ(O-H) of chemisorbed water molecules), asymmetric and symmetric γ(COO^-) at 1591 and 1483 cm^{-1}, respectively, and γ(C-N) at 1089 cm^{-1} (Fig. S11). The γ(C-S) signal could not be observed due to the bonding of the S atoms to the surface of AIGZS QDs.

The PL emission signals exhibit a clear redshift upon ligand exchange from 622 nm to 648 and 685 nm for AIGZS@GTMA and AIGZS@Gly-DTC QDs, respectively. The QDs are well dispersed in aqueous solution as demonstrated by DLS which shows hydrodynamic diameters of 14.6 ± 1.3 and 9.4 ± 1.8 nm for AIGZS@GTMA and AIGZS@Gly-DTC QDs, respectively, which indicate that the redshift originates from the changing of the environment around the dots and not from their aggregation (Fig. S12). The Zeta potential values of AIGZS@GTMA and AIGZS@Gly-DTC QDs are of -23.1 and -34.5 mV, respectively. Finally, the ligand exchange was accompanied by a slight decrease of the PL QY (from 48.3 to 43.7 and 37.4% for QDs capped with GTMA and Gly-DTC, respectively).

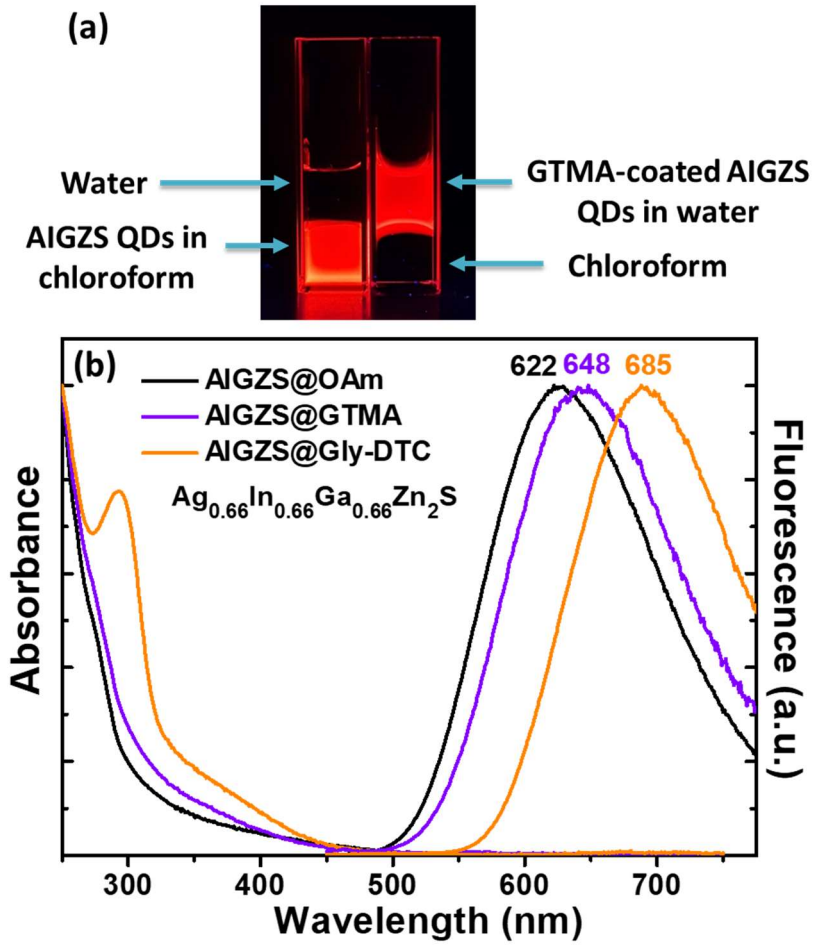

Fig. 6. (a) Digital photograph taken under UV light illumination of dispersions of AIGZS QDs before and after the ligand exchange with GTMA. (b) UV-visible and normalized PL emission spectra of AIGZS QDs capped with OAm and after their transfer into water using GTMA and Gly-DDTC ligands.

Conclusions

A single source molecular precursor synthesis was developed for the preparation of new quinary AIGZS QDs. The dots exhibit an average diameter of ca. 2 nm and their PL emission can be tuned from the green to the near-infrared by varying the Ag/In/Ga/Zn ratio. AIGZS QDs exhibit PL QYs up to 48.3%. The recombination of photogenerated electron-hole pairs occurs via surface-related trap states and intragap defect-related states and the PL lifetime could reach 915 ns for AIGZS QDs prepared with a Ag/In/Ga/Zn ratio of 1/0.5/0.5/1. These results show the high potential of AIGZS QDs as novel environmental-friendly fluorescent emitters.

CRediT authorship contribution statement

P. Galiyeva: Investigation, Writing - original draft. **H. Rinnert:** Investigation, Writing - review & editing. **L. Balan:** Investigation, Writing - review & editing. **H. Alem**: Investigation. **G. Medjahdi**: Investigation. **B. Uralbekov**: Supervision, Funding acquisition. **R. Schneider:** Supervision, Funding acquisition, Writing - review & editing.

Declaration of Competing Interest

The authors declare that they have no known competing financial interests or personal relationships that could have appeared to influence the work reported in this paper.

Acknowledgements

The authors thank the Bolashak International Scholarship of JSC "Center for International Programs" and the Kazakhstan ministry project of IRN AP08052719 for financial support.

Appendix A. Supplementary material

Supplementary data to this article can be found online at https://doi. org/xxx.

References

[1] W. M. Girma, M.Z. Fahmi, A. Permadi, M.A. Abate, J.Y. Chang, Synthetic strategies and biomedical applications of I–III–VI ternary quantum dots, J. Mater. Chem. B 5 (2017) 6193-6216.

[2] X. Bai, F. Purcell-Milton, Y.K. Gun'ko, Optical Properties, Synthesis, and Potential Applications of Cu-Based Ternary or Quaternary Anisotropic Quantum Dots, Polytypic Nanocrystals, and Core/Shell Heterostructures, Nanomaterials 9 (2019) 85.

[3] B. Chen, N. Pradhan, H. Zhong, From Large-Scale Synthesis to Lighting Device Applications of Ternary I–III–VI Semiconductor Nanocrystals : Inspiring Greener Material Emitters, J. Phys. Chem. Lett. 9 (2018) 435-445.

[4] M.D. Regulacio, M.-Y. Han, Multinary I-III-VI2 and I2-II-IV-VI4 Semiconductor Nanostructures for Photocatalytic Applications, Acc. Chem. Res. 49 (2016) 511-519.

[5] G. Xu, S. Zeng, B. Zhang, M.T. Swihart, K.-T. Yong, P.N. Prasad, New Generation Cadmium-Free Quantum Dots for Biophotonics and Nanomedicine, Chem. Rev. 116 (2016) 12234−12327.

[6] J. Kolny-Olesiak, H. Weller, Synthesis and Application of Colloidal $CuInS_2$ Semiconductor Nanocrystals, ACS Appl. Mater. Interfaces 5 (2013) 12221–12237.

[7] A.D.P. Leach, J.E. Macdonald, Optoelectronic Properties of $CuInS_2$ Nanocrystals and Their Origin, J. Phys. Chem. Lett. 7 (2016) 572–583.

[8] T. Torimoto, T. Kameyama, S. Kuwabata, Photofunctional Materials Fabricated with Chalcopyrite-Type Semiconductor Nanoparticles Composed of $AgInS_2$ and Its Solid Solutions, J. Phys. Chem. Lett. 5 (2014) 336–347.

[9] P. Galiyeva, H. Alem, H. Rinnert, L. Balan, S. Blanchard, G. Medjahdi, B. Uralbekov, R. Schneider, Highly fluorescent, colortunable and magnetic quaternary Ag–In–Mn–Zn–S quantum dots, Inorg. Chem. Front. 6 (2019) 1422–1431.

[10] M. Mrad, T. Ben Chaabane, H. Rinnert, L. Balan, J. Jasniewski, G. Medjahdi, R. Schneider, Aqueous Synthesis for Highly Emissive 3 Mercaptopropionic Acid- Capped AIZS Quantum Dots, Inorg. Chem. 59 (2020) 6220–6231.

[11] T. Kameyama, T. Takahashi, T. Machida, Y. Kamiya, T. Yamamoto, S. Kuwabata, T. Torimoto, Controlling the Electronic Energy Structure of $ZnS–AgInS_2$ Solid Solution Nanocrystals for Photoluminescence and Photocatalytic Hydrogen Evolution, J. Phys. Chem. C 119 (2015) 24740–24749.

[12] T. Torimoto, Y. Kamiya, T. Kameyama, H. Nishi, T. Uematsu, S. Kuwabata, T. Shibayama, Controlling Shape Anisotropy of $ZnS–AgInS_2$ Solid Solution Nanoparticles for Improving Photocatalytic Activity, ACS Appl. Mater. Interfaces 8 (2016) 27151–27161.

[13] M.R. Bergren, N.S. Makarov, K. Ramasamy, A. Jackson, R. Guglielmetti, H. McDaniel, High-Performance $CuInS_2$ Quantum Dot Laminated Glass Luminescent Solar Concentrators for Windows, ACS Energy Lett. 3 (2018) 520–525.

[14] Z. Wang, X. Zhang, W. Xin, D. Yao, Y. Liu, L. Zhang, W. Liu, W. Zhang, W. Zheng, B. Yang, H. Zhang, Facile Synthesis of Cu–In–S/ZnS Core/Shell Quantum Dots in 1-Dodecanethiol for Efficient Light-Emitting Diodes with an External Quantum Efficiency of 7.8%, Chem. Mater. 30 (2018) 8939–8947.

[15] W. Chung, H. Jung, C.H. Lee, S.H. Kim, Extremely high color rendering white light from surface passivated carbon dots and Zn-doped $AgInS_2$ nanocrystals, J. Mater. Chem. C 2 (2014) 4227-4232.

[16] D. Su, L. Wang, M. Li, S. Mei, X. Wei, H. Dai, Z. Hu, F. Xie, R. Guo, Highly luminescent water-soluble AgInS2/ZnS quantum dots-hydrogel composites for warm white LEDs, J. Alloys Compd. 824 (2020) 153896.

[17] A. Shamirian, O. Appelbe, Q. Zhang, B. Ganesh, S.J. Kronb, P.T. Snee, A toolkit for bioimaging using near-infrared $AgInS_2$/ZnS quantum dots, J. Mater. Chem. B 3 (2015) 8188-8196.

[18] M. Michalska, A. Florczak, H. Dams-Kozlowska, J. Gapinski, S. Jurga, R. Schneider, Peptide-functionalized ZCIS QDs as fluorescent nanoprobe for targeted HER2-positive breast cancer cells imaging, Acta Biomater. 35 (2016) 293-304.

[19] S.D. Perera, H. Zhang, X. Ding, A. Nelson, R.D. Robinson, Nanocluster seed-mediated synthesis of $CuInS_2$ quantum dots, nanodisks, nanorods, and doped Zn-$CuInGaS_2$ quantum dots, J. Mater. Chem. C 3 (2015) 1044-1055.

[20] W.-S. Song, J.-H. Kim, J.-H. Lee, H.-S. Lee, Y.R. Do, H. Yang, Synthesis of color-tunable Cu–In–Ga–S solid solution quantum dots with high quantum yields for application to white light-emitting diodes, J. Mater. Chem. 22 (2012) 21901-21908.

[21] Z.M. Hu, G.T. Fei, L.D. Zhang, Synthesis of green-to-red-emitting Cu-Ga-S/ZnS core/shell quantum dots for application in white light-emitting diodes, J. Lumin. 208 (2019) 18-23.

[22] S. Mei, G. Zhang, W. Yang, X. Wei, W. Zhang, J. Zhu, R. Guo, A facile route for highly efficient color-tunable Cu-Ga-Se/ZnSe quantum dots, Appl. Surf. Sci. 456 (2018) 876-881.

[23] J.-H. Kim, K.-H. Kim, S.-Y. Yoon, Y. Kim, S.-H. Lee, H.-S. Kim, H. Yang, Tunable Emission of Bluish Zn–Cu–Ga–S Quantum Dots by Mn Doping and Their Electroluminescence, ACS Appl. Mater. Interfaces 11 (2019) 8250-8257.

[24] D.-Y. Jo, D. Kim, J.-H. Kim, H. Chae, H.J. Seo, Y.R. Do, H. Yang, Tunable white fluorescent copper gallium sulfide quantum dots enabled by Mn doping, ACS Appl. Mater. Interfaces 8 (2016) 12291-12297.

[25] J.-H. Kim, B.-Y. Kim, E.-P. Jang, S.-Y. Yoon, K.-H. Kim, Y.R. Do, H. Yang, Synthesis of widely emission-tunable Ag-Ga-S and its quaternary derivative quantum dots, Chem. Eng. J. 347 (2018) 791-797.

[26] W.-J. Zhang, C.-Y. Pan, F. Coo, H. Wang, X. Yang, Bright violet-to-aqua-emitting cadmium-free Ag-doped Zn–Ga–S quantum dots with high stability, Chem. Commun. 54 (2018) 4176-4179.

[27] T. Kameyama, M. Kishi, C. Miyamae, D.K. Sharma, S. Hirata, T. Yamamoto, T. Hematsu, M. Vacha, S. Kuwabata, T. Torimoto, Wavelength-Tunable Band-Edge Photoluminescence of Nonstoichiometric Ag–In–S Nanoparticles via Ga^{3+} Doping, ACS Appl. Mater. Interfaces 10 (2018) 42844-42855.

[28] J. Song, Y. Zhang, Y. Dai, J. Hu, L. Zhu, X. Xu, Y. Yu, H. Li, B. Yao, H. Zhou, Polyelectrolyte-Mediated Nontoxic $AgGa_xIn_{1-x}S_2$ QDs/Low-Density Lipoprotein Nanoprobe for Selective 3D Fluorescence Imaging of Cancer Stem Cells, ACS Appl. Mater. Interfaces 11 (2019) 9884-9892.

[29] T. Torimoto, T. Adachi, K.-i. Okazaki, M. Sakuraoka, T. Shibayama, B. Ohtani, A. Kudo, S. Kuwabata, Facile Synthesis of ZnS−$AgInS_2$ Solid Solution Nanoparticles for a Color-Adjustable Luminophore, J. Am. Chem. Soc. 129 (2007) 12388-12389.

[30] M. Dai, S. Ogawa, T. Kamayama, K.-i. Okazaki, A. Kuda, S. Kuwabata, Y. Tsuboi, T. Torimoto, Tunable photoluminescence from the visible to near-infrared wavelength region of non-stoichiometric $AgInS_2$ nanoparticles, J. Mater. Chem. 22 (2012) 12851-12858.

[31] C.-M. Fan, M.D. Regulacio, C. Ye, S.H. Lim, Y. Zheng, Q.-H. Xu, A.-W. Xu, M.-Y. Han, Colloidal synthesis and photocatalytic properties of orthorhombic $AgGaS_2$ nanocrystals, Chem. Commun. 50 (2014) 7128-7131.

[32] S. Wei, Y. Liu, M. Ma, Y. Wu, L. Huang, D. Pan, Thin-shell CdSe/ZnCdS core/shell quantum dots and their electroluminescent device application, J. Mater. Chem. C 6 (2018) 11104-11110.

[33] S. Shen, Y. Zhang, L. Peng, B. Xu, Y. Du, M. Deng, H. Xu, Q. Way, Generalized synthesis of metal sulfide nanocrystals from single-source precursors: size, shape and chemical composition control and their properties, CrystEngComm 13 (2011) 4572-4579.

[34] J.C. Bear, N. Hollingsworth, A. Raffey, P.D. McNaughter, A.G. Mayes, T.J. Macdonald, T. Nann, W.H. Ng, A.J. Kenyon, G. Hogarth, I.P. Parkin, Doping Group IIB Metal Ions into Quantum Dot Shells via the One-Pot Decomposition of Metal-Dithiocarbamates, Adv. Optical Mater. 3 (2015) 704-712.

[35] D. Chen, F. Zhao, H. Qi, M. Rutherford, X. Peng, Bright and Stable Purple/Blue Emitting CdS/ZnS Core/Shell Nanocrystals Grown by Thermal Cycling Using a Single-Source Precursor, Chem. Mater. 22 (2010) 1437-1444.

[36] J. Cai, S; Wang, K. Zhu, Y. Wu, L. Zhou, Y. Zhang, Q. Wu, X. Wang, Z. Hu, Synthesis of alloyed $Zn_{1-x}Mn_xS$ nanowires with completely controlled compositions and tunable bandgaps, RSC Adv. 8 (2018) 374-379.

[37] Y. Wang, J. Wu, J. Zheng, R. Jiang, R. Xu, Ni^{2+}-doped $Zn_xCd_{1-x}S$ photocatalysts from single-source precursors for efficient solar hydrogen production under visible light irradiation, Catal. Sci. Technol. 2 (2012) 581-588.

[38] Y. Wei, J. Yang, J.Y. Ying, Reversible phase transfer of quantum dots and metal nanoparticles, Chem. Commun. 46 (2010) 3179.

[39] F. Dubois, B. Mahler, B. Dubertret, E. Doris, C. Mioskowski, A Versatile Strategy for Quantum Dot Ligand Exchange, J. Am. Chem. Soc. 129 (2007) 482-483.

[40] R.G. Pearson, Hard and soft acids and bases, HSAB, part 1: Fundamental principles, J. Chem. Educ. 45 (1968) 581-587.

[41] W. Liu, Low temperature synthesis of hexagonal phase ZnS nanocrystals by thermolysis of an air-stable single-source molecular precursor in air, Mater. Lett., 60 (2006) 551-554.

[42] A.C. Costa Jr, G.F. Ondar, O. Versiane, J.M. Ramos, T.G. Santos, A.A. Martin, L. Raniero, G.G.A. Bussi, C.A. Tellez Soto, DFT: B3LYP/6-311G (d, p) vibrational analysis of bis-(diethyldithiocarbamate)zinc (II) and natural bond orbitals, Spectrochim. Acta A Mol. Biomol. Spectrosc. 105 (2013) 251-258.

[43] R. Vogel, P. Hoyer, H. Weller, Quantum-Sized PbS, CdS, Ag_2S, Sb_2S_3, and Bi_2S_3 Particles as Sensitizers for Various Nanoporous Wide-Bandgap Semiconductors, J. Phys. Chem. 98 (1994) 3183-3188.

[44] S. Khanchandani, S. Kundu, A. Patra, A.K. Ganguli, Band Gap Tuning of ZnO/In_2S_3 Core/Shell Nanorod Arrays for Enhanced Visible-Light-Driven Photocatalysis, J. Phys. Chem. C 117 (2013) 5558-5567.

[45] N. Zhou, L. Gan, R. Yang, F. Wang, L. Li, Y. Chen, D. Li, T. Zhai, Nonlayered Two-Dimensional Defective Semiconductor γ-Ga_2S_3 toward Broadband Photodetection, ACS Nano 13 (2019) 6297-6307.

[46] B. Mao, C.-H. Chuang, C. McCleese, J. Zhu, C. Burda, Near-Infrared Emitting $AgInS_2/ZnS$ Nanocrystals, J. Phys. Chem. C 118 (2014) 13883-13889.

[47] S. Jeong, H.C. Yoon, N.S. Han, J.H. Oh, S.M. Park, B.K. Min, Y.R. Do, J.K. Song, Band-Gap States of $AgIn_5S_8$ and $ZnS–AgIn_5S_8$ Nanoparticles, J. Phys. Chem. C 121 (2017) 3149-3155.

[48] O. Stroyuk, A. Raevskaya, F. Spranger, O. Selyshchev, V. Dzhagan, S. Schulze, D.R.T. Zahn, A. Eychmüller, Origin and Dynamics of Highly Efficient Broadband Photoluminescence of Aqueous Glutathione-Capped Size-Selected Ag–In–S Quantum Dots, J. Phys. Chem. C 122 (2018) 13648-13658.